Surface Science 222 (1989) 464–476
North-Holland, Amsterdam

ATOM-SCATTERING STUDY OF Ar^+ ION DAMAGED GaAs(110)

B.D. WEAVER [1], D.R. FRANKL [1], Rik BLUMENTHAL [2] and N. WINOGRAD [2]

Departments of Physics [1] and Chemistry [2], The Pennsylvania State University, 104 Davey Laboratory, University Park, PA 16802, USA

Received 18 April 1989; accepted for publication 27 June 1989

Helium atom scattering has been used to probe the surface damage created on GaAs(110) by Ar^+ ion bombardment. The scattering cross section, Σ, of a single monovacancy is found to be ~ 150 Å^2. The average number of defects comprising isolated impact craters, estimated from the scattering cross section per crater, is found to decrease with increasing crystal temperature during bombardment. This decrease occurs during or shortly following the bombardment event, and is different from simple thermal annealing. We propose that thermal accommodation of target adatom energy, which requires the number of adatom hops before freezing to increase with increasing crystal temperature, increases the adatom–vacancy recombination probability. Increasing the ion energy from 600 to 2400 eV does not change the cross section per single crater, but apparently impedes the probability of recombination.

1. Introduction

Ion-beam induced lattice damage is an ubiquitous limitation in the processing of semiconductor devices. For example, the creation of lattice vacancies, adatoms and other surface defects influence electrical conductivity [1]. The diffusion rates and spatial distribution of ion-implanted dopants limit device size reduction and allowable processing temperatures. This damage is also a significant factor in ion-beam plating [2], radiation-enhanced diffusion [3] and ion beam-induced epitaxial growth [4].

It is an experimental challenge to gain insight into the dynamical aspects of the damage process. If the damage sites are large enough, as perhaps when created by rare "mega-events" [5], they can be directly imaged by electron or scanning tunneling microscopy [6–8], or field ion microscopy [9]. Spectroscopic studies of bombarded solids using low energy electron diffraction (LEED) [10,11], Auger electron spectroscopy [12], X-ray photoelectron spectroscopy [13] and low energy ion scattering [14] have been limited to highly damaged surfaces (a few to a few dozen sputtered monolayers). Only a very few studies have been presented in which smaller amounts of damage have been probed. The experimental conditions in these cases [7–9] resulted in

0039-6028/89/$03.50

modestly high-yield bombardment events (typically > 10 ejected atoms per impact). To our knowledge, only one previous work, an atom-scattering study of 600 eV Ar^+ ion-bombarded Pt{111} [15], has addressed a situation in which the yield is of order unity.

In this work, we present the results of an atom-scattering study of Ar^+ ion-damaged GaAs(110). Atom-scattering is particularly advantageous for the study of surface damage, since even monoatomic defects exert a large influence on the scattering potentials and hence the scattering amplitudes [16,17]. Ion fluences lower than one ion per hundred surface atoms can cause surface damage that significantly decreases the scattering intensity. This sensitivity allows measurement of the scattering cross section of an average isolated impact site (a "crater") and estimation of its configuration, even when this configuration consists of only one defect. We have explored the changes in this configuration due to variations in sample temperature and incident ion energy. In addition to normal thermal annealing, a temperature-dependent bombardment-related healing process has been observed. We suggest a mechanism in the form of temperature-dependent accommodation of target adatom energy.

2. Experimental

The beam source, analysis chamber and sample preparation technique have all been described elsewhere [18,19], so only a brief summary is given here. The 16.8 meV He-beam is formed by supersonic expansion of low temperature (80 K), high pressure (70 atm) helium gas through a small aperture (five microns) into a vacuum chamber, where a narrow beam is extracted by skimming. In the two following differential pumped stages, the beam is modulated at a frequency of 400 Hz [20], and collimated to yield a divergence half angle of 0.05°, giving a 1.9 mm beam diameter at the crystal. The cooling effect of the supersonic expansion results in a velocity distribution whose full width at half-maximum (FWHM) is about 1.4%. The beam flux at the detector is $\sim 10^{19}$ atoms per steradian per second. The angle ($< 0.5°$) subtended by the circular detector aperture at the crystal is smaller than the FWHM of all measured peaks, so no deconvolution is required [21,22]. For all experiments, the helium beam was incident along the (001) surface azimuth, i.e., perpendicular to the atomic rows of the (110) surface. Azimuthal alignment is set by maximizing the higher order diffraction intensities, and by LEED. The base pressure of the analysis chamber is less than 8×10^{-11} Torr, but during operation rises to about 1.5×10^{-10} Torr. At these pressures, the specular reflection from an initially clean surface remains observable for two to three days, implying that surface contamination is not a significant problem.

Crystals are bombarded with Ar^+ ions from a differentially pumped ion source [19]. The flux and uniformity of the ion beam are measured in situ with a flat phosphor-coated copper plate. Below about 2 keV, the yield of secondary electrons is too small to cause a noticeable error in the measured ion current [23], which was stable to about 2% during the experiments. The ion beam was incident along the surface normal. In most cases the dose rate was 4×10^{10} ions/cm$^2 \cdot$ s, or approximately 5×10^{-5} ions per surface atom per second.

The diffracted beams from a clean, freshly annealed surface were first measured at fixed crystal temperature T to provide clean-surface peak intensities $I_0(T)$. This measurement was performed by scanning the crystal polar axis at constant total scattering angle θ_t. Most data were obtained at $\theta_t = 136.4°$, with incident and final scattering angles $\theta_i = \theta_f = 68.2°$, because this geometry results in the largest specular reflection, about 4% of the direct beam. Similar scans of the fourth order peak at $\theta_t = 84.6°$ around $\theta_i = 74.0°$ were also performed. The surface was then damaged by ion-bombardment, and the peak specular reflection was monitored during one of two types of experiment. In the first, the peak intensity of a sample bombarded at 300 K was measured as a function of crystal temperature during a programmed annealing cycle. In the second type of experiment, the peak intensity at fixed temperature was measured as a function of ion fluence. This experiment was performed at crystal temperatures between 300 and 700 K, and for ion energies between 600 and 2400 eV.

3. Results and discussion

The effect of ion bombardment on specular reflection is illustrated in fig. 1. Note that increasing ion exposure attenuates the peak height of the reflected beam but does not significantly alter its lineshape. The amplitude of the inelastic "wings", which are presumably due to surface phonons [24], is also attenuated uniformly with increasing ion fluence. As the sample is irradiated, the background level (measured several degrees away from the peak) increases almost without structure from less than 2 to about 3% of the clean surface peak height. To a good approximation, then, atom-scattering from ion-induced defects occurs isotropically (i.e., is diffuse), so the ratio of the peak intensity $I(T)$ to the clean-surface peak intensity represents the probability of scattering from an undamaged portion of the surface.

The programmed annealing curves $I(T)/I_0(T)$ versus T are shown in fig. 2. The normalized intensity remains fixed for T less than about 600 K, regardless of heating rate or initial surface quality. This observation implies that the surface morphology is also fixed, and that thermal annealing is not occurring. The damage curves (normalized intensity versus ion fluence) for 600

where the defect coverage Θ is

$$\Theta = n_d/n_s, \tag{3}$$

n_s being the surface atomic density.

In the case of ion bombardment, the surface damage resulting from an impact is expected to be a defect cluster or "crater" centered about the impact site. We designate the average scattering cross section of an entire crater as Σ'. For small f, where the average separation between impact sites is large, the peak intensity can be written in analogy to eq. (2) as

$$I(T)/I_0(T) = 1 - n'_d\Sigma' \tag{4a}$$

$$= 1 - \Theta' n_s \Sigma' \tag{4b}$$

$$= 1 - f\Sigma', \tag{4c}$$

where n'_d is the density of impact sites, and

$$\Theta' = n'_d/n_s. \tag{5}$$

The maximum fluence of 8.8×10^{12} ions/cm^2 shown in the insert of fig. 3, corresponds to 1 ion impact per 100 surface atoms ($\Theta' = 0.01$). Under these low-fluence conditions, most craters are well-isolated from their nearest-neighbors, so eq. (4c) is immediately applicable to determining Σ' from the slopes of the curves. As illustrated in fig. 4, we find that these values depend upon the sample temperature during bombardment, decreasing from 350 Å^2 at 300 K to 150 Å^2 for $T \geq 600$ K. The simplest explanation for this dependence would be that thermal annealing allows motions that effectively reduce Σ'. This could occur, for example, by the clustering of defects within craters, or the clustering of craters into groups whose blemished areas overlap. However, neither the temperature-programmed thermal annealing curves of fig. 2 nor the one-hour annealing shown in fig. 3 indicate sufficiently rapid changes to account for the observed temperature dependence. Furthermore, annealing at a higher temperature (500 K) does not reverse the damage due to bombardment at a lower temperature (300 K). Thus the thermal annealing rates at low temperatures are far too small to cause the observed temperature dependence of Σ'.

Thus, although Σ' is obviously dependent upon T during bombardment, it is only very weakly dependent upon T after bombardment. This means that the processes leading to the temperature-dependent value of Σ' must occur during or shortly after the ion impact, following which the average crater morphology changes only slowly via thermal annealing. This is a surprising result, because many hundreds of eV are imparted to the crystal in a single impact, yet the crater structure depends markedly on the much smaller thermal energy during the event. We term this phenomenon "bombardment-related healing".

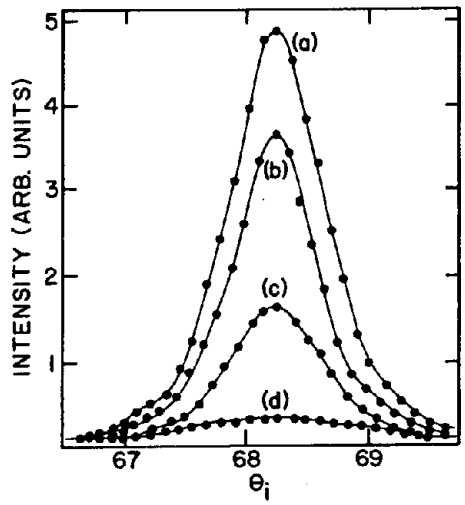

Fig. 1. Specular reflection profile around $\theta_i = 68.2°$ for (a) a clean surface, and ion doses of (b) 7×10^{12} ions/cm^2, (c) 4×10^{13} ions/cm^2, and (d) 10^{14} ions/cm^2.

eV Ar^+ ions are shown in fig. 3 for various values of T. The vertical increase in $I(T)/I_0(T)$ at the end of each curve ($f = 8.8 \times 10^{13}$ ions/cm^2) results from a one-hour anneal, in which the scattering intensity is monitored continuously after the ion beam is turned off. Again, no thermal annealing is observed below 600 K. The damage curve for the $(\bar{4}0)$ diffraction peak, also shown for $T = 300$ K in fig. 3, exhibits the same attenuation behavior as the specular reflection peak.

The information contained in these figures can be quantitatively interpreted by considering the effect of single imperfections on peak intensities. Each defect in a solid surface locally destroys the two-dimensional periodicity and

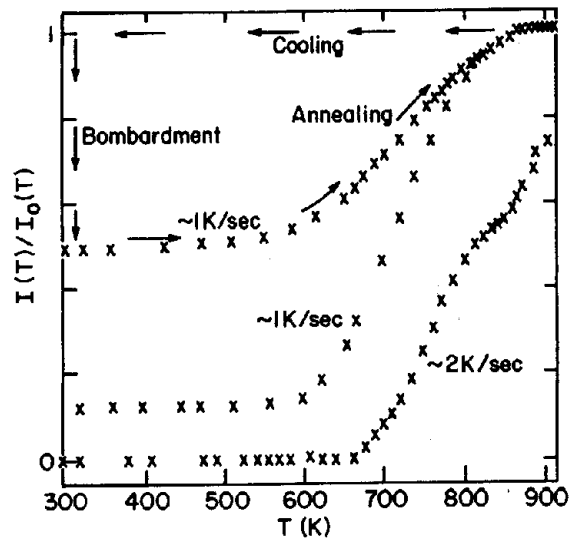

Fig. 2. Programmed annealing curves: normalized specular intensity for $\theta_i = 68.2°$ versus sample temperature for fixed rates of heating. The arrows indicate a typical annealing cycle.

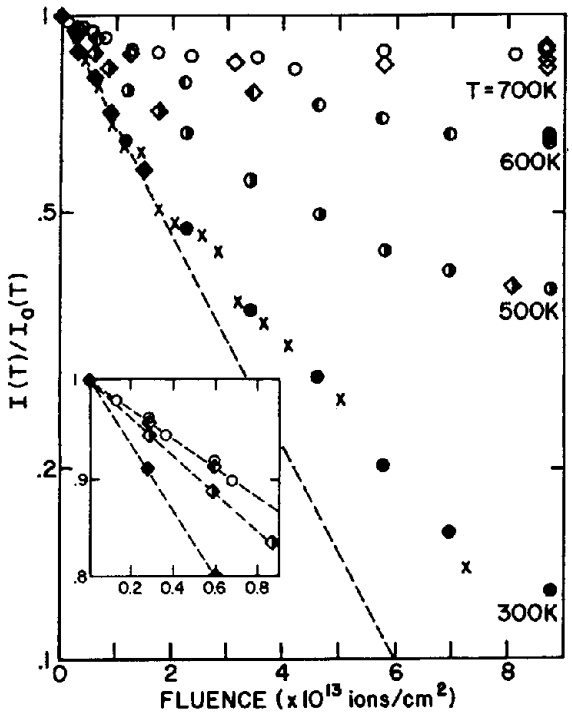

Fig. 3. Normalized specular intensity versus ion fluence for $\theta_i = 68.2°$ and different sample temperatures T. Solid symbols: $T = 300$ K; right-solid symbols: $T = 500$ K; left-solid symbols: $T = 600$ K; open symbols: $T = 700$ K. crosses: $(\bar{4}0)$ reflection, $\theta_i = 74.0°$. The dashed line is the prediction of eq. (12) for $\Sigma' = 350$ Å^2. The vertical increases at $f = 8.8 \times 10^{13}$ ions/cm^2 represent the degree of thermal annealing in one hour.

perturbs the equipotentials of the atom–surface interaction [16,17]. For the purposes of atom-scattering, an isolated defect can be thought of as producing a larger "blemish" of area Σ (the "scattering cross-section"), within which the scattering is diffuse. With a given fraction P of the surface area covered by such blemishes, the measured signal $I(T)$ is simply

$$I(T)/I_0(T) = 1 - P. \tag{1}$$

The manner in which P increases with the surface defect density n_d depends upon the size, shape, and proximity of the blemishes. A defect's extensive perturbation of the low energy scattering contours leads to cross sections that are generally of the order of 100 Å^2 [15,25,26]. This large cross-section renders atom-scattering sensitive to extremely low defect coverages. It is also sensitive to the lateral distribution of defects, because the blemishes due to two defects closer to each other than roughly 5–6 Å will overlap, and their combined cross section will be less than 2Σ. For the case of widely-separated defects where no overlap occurs,

$$I(T)/I_0(T) = 1 - n_d\Sigma = 1 - \Theta n_s\Sigma, \tag{2}$$

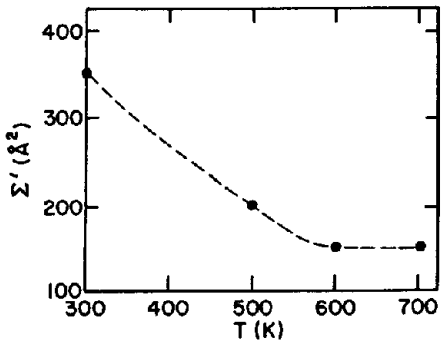

Fig. 4. The value of Σ' versus T. The Σ' values were obtained from eq. (4c) and the data of fig. 3.

According to fig. 4, as T increases, Σ' levels out at about 600 K. Since the scattering cross section of an individual defect is not temperature-dependent [27], this shows that the physical size of the craters decreases with increasing temperature, and eventually becomes constant. The smallest possible crater size is determined by the desorption yield Y, which for 600 eV Ar^+ ion-bombarded GaAs(110) is 1 [28]. Thus it is reasonable to assume that above about 600 K, most of the initial bombardment damage within each crater reheals, leaving a single monovacancy whose scattering cross section is $\Sigma_{\text{mono}} \approx 150$ Å^2. This value is in excellent agreement with the scattering cross section of a monovacancy on Pt{111} [15]. The large value of Σ_{mono} has been explained in terms of the significant van der Waals interaction between a scattering atom and a highly polarizable vacancy [16].

The larger cross sections for $T < 600$ K imply that there are a larger number of residual defects per crater. Since the average sputtering yield is not strongly dependent on temperature [29], the additional surface defects within a crater must occur approximately in pairs (e.g. one target adatom per additional vacancy), and although the exact location of these defects within a crater is unknown, their number can be estimated. By drawing variously configured clusters of defects on a GaAs(110) surface mesh and embellishing each defect with a 150 Å^2 blemish area, we find that to yield $\Sigma' = 200$ Å^2 (the value at 500 K), the total number of surface defects per crater, n_t, must be between 1.3 and 3, depending on their proximity and the corresponding amount of cross-sectional overlap. For $T = 300$ K, the number is $2.3 < n_t < 5$. (We have approximated the scattering cross section of a target adatom as equal to that of a monovacancy.) To obtain $Y = 1$, the average number of vacancies per crater, n_v, must exceed the number of target adatoms n_a by one, while $n_t = n_a + n_v$. Thus for 300 K, we find $0.7 < n_a < 2$. At the higher temperatures, n_a is reduced by the bombardment-related healing processes mentioned above. For 500 K, $0.2 < n_a < 1$, and above 600 K, $n_a = 0$.

The values of n_a are within range of those predicted by molecular dynamics simulations [30], but are somewhat lower than those apparent from atomically

resolved STM images and high resolution TEM images of similar types of defects [7–9]. We believe this latter discrepency arises in part since the direct imaging methods are focussing directly on high-action impact points where the ejection yield is greater than 30 atoms/incident ion. The atom-scattering probe discussed here yields a more typical n_a value associated with an impact event with a desorption yield closer to 1.

There are various ways in which n_a can decrease. First, adatoms can be lost at step edges. This is unlikely to have a major effect on Σ', though, because only a small fraction of craters will be close enough to steps that their adatoms can migrate to them in the short interval surrounding the ion impact. A more likely possibility is that adatoms recombine with nearby vacancies. For low fluences, this must occur within isolated craters because the inter-crater distance is too large. This recombination reduces the physical size of a crater, thereby reducing Σ'. Since vacancy hopping requires the breaking of bonds, while the hopping of newly-created, energetic target adatoms does not, the increasing recombination probability most likely results from an increasing number of adatom hops before freezing. The mechanism for this enhancement must arise from the thermal accommodation of the adatom energy. Assuming a constant accommodation coefficient α, an adatom's temperature after j hops is [31]

$$T_j = [T_0 - T][1 - \alpha]^j + T, \tag{6}$$

where T_0 is the initial adatom temperature. Hopping effectively ceases when the average time per hop exceeds the experiment duration. For this to occur, the adatom temperature T_j must fall below some "freezing temperature" T_f. Thus the maximum number of hops is obtained from eq. (6) as

$$j_f = \frac{\ln(T_f - T) - \ln(T_0 - T)}{\ln(1 - \alpha)}. \tag{7}$$

The temperature behavior of both the scattering cross section and the annealing curves suggests that T_f is ~ 600 K. Molecular dynamics simulations suggest that target adatom energies are on the order of 1 eV (10^4 K) [32]. We consider first that the energy contributed to the sample by the ion is dissipated before adatom hopping occurs, so that the crystal temperature T is given by its equilibrium value. Then an arbitrarily assumed value of 0.7 for α yields $j_f = 3$ at 300 K, 4 at 500 K, and 8 at 599 K. Other combinations of the parameters can yield a higher degree of T-dependence, especially if α is allowed to decrease with increasing T, as is known to be the case for Xe on W [31].

Thus it is likely that the strong dependence of the cluster size and cross section on the sample temperature is due to the T-dependent adatom energy accommodation. It is known that the crystal lattice remains locally agitated for

about a picosecond after the collision [5,32], so in this vicinity, target adatoms experience crystal temperatures temporarily higher than T. Regardless of their initial energy or the crystal's equilibrium temperature, then, adatoms should always be able to make a few jumps before freezing. Although this will reduce the degree of temperature dependence of j_f, it evidently does not completely remove it.

The same process qualitatively predicts the intensity behavior at higher fluences. For single defects, the probability that a given lattice cell contains a defect is Θ. Each defect causes an area Σ, or equivalently, the surrounding $n_s\Sigma$ cells, to scatter diffusely. Thus a given cell scatters coherently if neither it nor any of the $n_s\Sigma$ neighboring cells contain a defect. This results in an intensity [25]

$$I(T)/I_0(T) = (1-\Theta)^{n_s\Sigma}. \tag{8}$$

In the absence of inter-crater interactions, a similar argument would apply to the ion bombardment craters, so that

$$I(T)/I_0(T) = (1-\Theta')^{n_s\Sigma'}. \tag{9}$$

If we consider that a new (though possibly overlapping) crater is formed whenever an incident ion strikes a previously unimpacted cell, the probability of which is $(1-\Theta')$, then

$$n_s\, d\Theta' = (1-\Theta')\, df, \tag{10}$$

so that

$$\Theta' = 1 - \exp(-f/n_s). \tag{11}$$

Inserting eq. (11) into eq. (9) yields

$$I(T)/I_0(T) = \exp(-f\Sigma'). \tag{12}$$

This exponential behavior reduces to eq. (4) for small values of f.

Experimentally, it is obvious from fig. 3 that at higher fluences all damage curves fall above the exponential curves, indicating the presence of inter-crater "healing" interactions. This is an expected result of the adatom hopping model, because as the ion fluence increases, impact craters become closer, and temporarily mobile adatoms are able to undergo inter-crater as well as intra-crater recombinations. This increases the net recombination probability, reduces the effective amount of damage per ion impact, and causes the scattering intensity to be larger than the value expected for overlapping but noninteracting craters.

For the purpose of illustrating the general behavior of the surface healing mechanism and summarizing the net intensity behavior, we performed a series of computer simulations, wherein 10^4 lattice cells are constructed to mimic the GaAs(110) surface, and are disrupted by various ion fluences. The initial

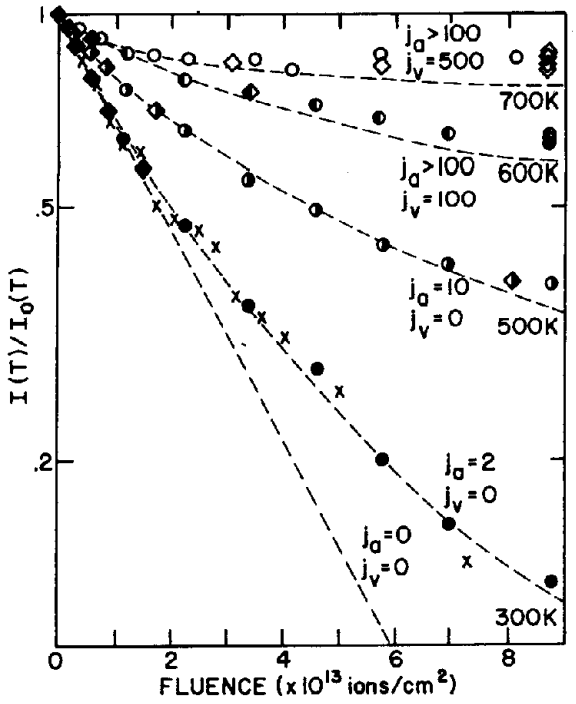

Fig. 5. Normalized specular intensity versus ion fluence for $\theta_i = 68.2°$. The dashed lines are the result of computer simulations. j_a = maximum number of target adatom jumps before freezing. j_v = number of vacancy jumps during experiment.

damage caused by each impact comprises two vacancies and a target adatom ($n_t = 3$ or $n_a = 1$). The first vacancy is placed randomly, while for consistency with molecular dynamics simulations [30,32], the second vacancy and the adatom are located randomly up to three unit cells away. Once placed, the target adatom is allowed a fixed number of jumps, j_a, before freezing. The direction of these jumps is random unless the adatom is within one hop of an existing defect, in which case it moves preferentially and either recombines with a vacancy or forms an adatom cluster. At sufficiently high temperature, not only the adatoms but also the vacancies are allowed a fixed number of jumps, j_v. Once a given fluence is achieved, 150 Å^2 blemishes are drawn around each defect, and the normalized scattering intensity is determined from the fraction of the surface area not covered by blemish areas. The best-fit results are shown in fig. 5. The value of $j_a = 0$ leads to the exponential decay predicted by eq. (12). The value of $j_a = 2$ fits the 300 K data nearly perfectly, as does $j_a = 10$ for $T = 500$ K. Since no more than a qualitative description is possible using this procedure, the sensitivity of these numbers to the initial site configuration was not extensively explored. Considering the simplicity of this model, the results are remarkably good.

The result of varying the ion energy is shown in fig. 6 for $T = 300$ K. The value of Σ' is constant for ion energies between 600 and 2400 eV, but the damage curves show an increasing tendency toward exponentiality as the ion

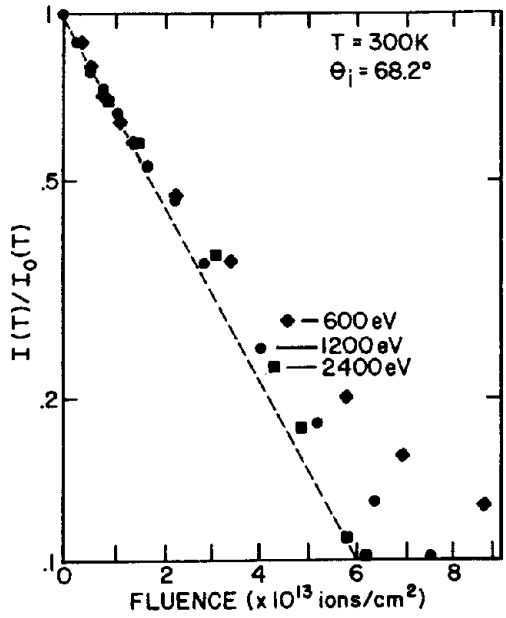

Fig. 6. Normalized specular intensity versus ion fluence for various Ar^+ energies. Dashed line: prediction of eq. (12) for $\Sigma' = 350$ Å^2.

energy increases. A possible explanation for this observation is that since incident ion trajectories are along a bulk channeling direction, increased ion energies result in nearly identical surface blemishes while causing a greater amount of subsurface damage and impeding inter-crater interactions. Proof of this conjecture must be forthcoming from some other technique, however, since atom-scattering probes only the outermost layer.

4. Summary of conclusions

The extreme sensitivity of atom-scattering to surface defects allows the morphology of ion-damaged surfaces to be explored at very low fluences, where damage centers are well-isolated. We hypothesize the following response of the GaAs(110) surface to 600 eV Ar^+ ion bombardment. At $T = 300$ K, an average impact results in 2.3 to 5 defects, approximately one of which is a target adatom, which can make a few jumps before freezing. At 500 K, the initial surface damage is most likely the same, but the decreased efficiency in the accommodation of adatom energy allows more adatom jumps before freezing. The result is a higher degree of surface healing. Above about 600 K, adatoms remain mobile until recombining with vacancies or forming adatom clusters. At and above 700 K, the dominant surface healing process becomes thermal annealing.

This mechanism suggests an important refinement for future generations of molecular dynamics calculations, since it is likely to play a dominant role in

radiation-enhanced epitaxial crystal growth [3]. It is certainly relevant to the undesired intermixing of target and film species [2] in ion beam deposition, since the migration of target adatoms can be minimized by proper selection of the crystal temperature. Although the underlying physics of the phenomenon described here is far from new, the atomistic nature of the results promise new applications for atom-scattering. Nonetheless, it would be interesting to see these results confirmed and extended to other surfaces, for example by an STM examination of any very low-yield process.

Acknowledgements

It is a pleasure to acknowledge discussions with Professor B.J. Garrison. Conversations with K.P. Caffey, S.K. Donner, T.T. Tsong, and R.P. Webb were valuable. Special consideration is due to the late D.E. Harrison, Jr. for his friendly encouragement and advice. This work was supported in part by the NSF grants DMR-8718771 and CHE-8608870, ONR Contract N00014-86-K-0190, and the IBM corporation.

References

[1] D. Stark, Surface Sci. 189 (1987) 1111.
[2] H. Westendorp, Z.L. Wang and F.W. Saris, Nucl. Instr. Methods 194 (1982) 453.
[3] J. Linnros, B. Svenson and G. Holmén, Phys. Rev. B 30 (1984) 3629.
[4] W.F. Egelhoff, Jr. and I. Jacob, Phys. Rev. Letters 62 (1989) 921.
[5] R.P. Webb and D.E. Harrison, Jr., Phys. Rev. Letters 50 (1983) 1478.
[6] D. Cherns, Phil. Mag. 36 (1977) 1429.
[7] S.R. Bhattacharya, D. Ghose, D. Basu and S.B. Karmohapatro, J. Vacuum Sci. Techol. A 5 (1979 33;
W. Jager and K.L. Merkle, Phil. Mag. A 57 (1988) 479.
[8] I.H. Wilson, N.J. Zheng, U. Knipping and I.S.T. Tsong, Phys. Rev. B 38 (1988) 8444;
I.H. Wilson, N.J. Zheng, U. Knipping and I.S.T. Tsong, Appl. Phys. Letters 53 (1988) 2039.
[9] D.H. Seidman, M.J. Current, D. Pramanik and C.-Y. Wei, Nucl. Instr. Methods 182/183 (1981) 477.
[10] R.L. Jacobson and G.K. Wehner, J. Appl. Phys. 36 (1965) 2674.
[11] H.E. Farnsworth and K. Hayek, Surface Sci. 8 (1967) 35.
[12] J.P. Petrakian and P. Renucci, Surface Sci. 195 (1988) 151.
[13] D.A. Asbury and G.B. Hoflund, Surface Sci. 199 (1988) 552.
[14] L.K. Verheij, J.A. van den Berg and D.G. Armour, Surface Sci. 122 (1982) 216.
[15] B. Poelsema, K. Lenz, L.S. Brown, L.K. Verheij and G. Comsa, Surface Sci. 162 (1985) 1011.
[16] E. Zaremba, Surface Sci. 151 (1985) 91.
[17] A.T. Yinnon, R. Kosloff, R.B. Gerber, B. Poelsema and G. Comsa, J. Chem. Phys. 88 (1988) 3722.
[18] B.D. Weaver and D.R. Frankl, Rev. Sci. Instr. 58 (1987) 2115.
[19] R. Blumenthal, S.K. Donner, J.L. Herman, R. Trehan, K.P. Caffey, E. Furman, N. Winograd and B.D. Weaver, J. Vacuum Sci. Technol. B 6 (1988) 1444.

[20] B.D. Weaver and D.R. Frankl, Rev. Sci. Instr. 59 (1988) 92.
[21] G. Comsa and R. David, Surface Sci. Rept. 5 (1985) 145.
[22] B.J. Hinch, D.R. Frankl and W. Allison, Surface Sci. 180 (1987) 371.
[23] R.A. Baragliola, E.V. Alonso, J. Ferron and A. Oliva-Florio, Surface Sci. 90 (1979) 240.
[24] M.J. Cardillo, G.E. Becker, S.J. Sibener and D.R. Miller, Surface Sci. 107 (1981) 469.
[25] B. Poelsema, R.L. Palmer and G. Comsa, Surface Sci. 136 (1984) 1.
[26] B. Poelsema, L.K. Verheij and G. Comsa, Phys. Rev. Letters 49 (1983) 2410.
[27] B. Poelsema, L.K. Verheij and G. Comsa, Surface Sci. 148 (1984) 117.
[28] A. Benninghoven, F.G. Rudenauer and H.W. Werner, in: Secondary Ion Mass Spectrometry (Wiley, New York, 1987).
[29] H.E. Roosendaal, in: Sputtering by Particle Bombardment I, Ed. R. Behrisch (Springer, Berlin, 1981) p. 240.
[30] R.P. Webb and D.E. Harrison, Jr., Radiation Effects Letters 86 (1983) 15; Nucl. Instr. Methods 218 (1983) 697.
[31] E.W. Mueller and T.T. Tsong, in: Field Ion Microscopy (Elsevier, New York, 1969) pp. 30–36.
[32] D.E. Harrison, Jr., Crit. Rev. Solid State and Mater. Sci. 14 (1988) 15.